Pure Appl. Chem., Vol. 82, No. 6, pp. 1259–1272, 2010.
doi:10.1351/PAC-CON-09-09-38

Synthesis of carbon nanotubes by plasma-enhanced chemical vapor deposition in an atmospheric-pressure microwave torch*

Lenka Zajíčková[1,‡], Ondrej Jašek[1], Marek Eliáš[1], Petr Synek[1], Lukáš Lazar[1], Oldřich Schneeweiss[2], and Renáta Hanzlíková[3]

[1]Department of Physical Electronics, Faculty of Science, Masaryk University, Kotlarska 2, 611 37 Brno, Czech Republic; [2]Institute of Physics of Materials, Academy of Sciences of the Czech Republic, Zizkova 22, 616 62 Brno, Czech Republic; [3]Institute of Scientific Instruments, Academy of Sciences of the Czech Republic, Kralovopolska 147, 612 64 Brno, Czech Republic

Abstract: There are many different techniques for the synthesis of carbon nanotubes (CNTs), and plasma technologies experience a significant competitor in thermal chemical vapor deposition (CVD) processes. A particular process is, therefore, selected according to the specific requirements of an application, which clearly differ for the development of composites as compared to nanoelectronics, field emission, displays, sensors, and the like. This paper discusses the method for the synthesis of CNTs using an atmospheric-pressure microwave (MW) torch. It was successfully applied in the fast deposition of multiwalled nanotubes (MWNTs) on a substrate without the necessity of any vacuum or heating equipment. Dense straight-standing nanotubes were prepared on Si substrates with and also without barrier SiO_x layer. Therefore, it was possible to produce CNTs directly on conductive Si and to use them as an electron-emitting electrode of the gas pressure sensor. The CNTs grown in MW torch were also used to create a gas sensor based on the changes of electrical resistance measured between two planar electrodes connected by the CNTs.

Keywords: carbon nanotubes; catalyst; microwave torch; plasma-enhanced chemical vapor deposition; scanning electron microscopy.

INTRODUCTION

Chemical vapor deposition of carbon nanotubes

Chemical vapor deposition (CVD) has been widely used for the synthesis of carbon nanotubes (CNTs) in recent years. This method can be used for volume production as well as direct growth of supported aligned CNTs. It is widely acknowledged that transition-metal catalysts are needed for single-walled nanotubes (SWNTs), multiwalled nanotubes (MWNTs), and carbon nanofiber (CNF) growth by CVD [1]. The general growth mechanism proceeds through the dissociation of carbon-containing molecules catalyzed by the transition-metal nanoparticles (NPs). It was suggested by Vinciguerra et al. [2] that diffusion of carbon into metal NPs is not essential for SWNT nucleation in catalytic CVD. However, some

*Paper based on a presentation at the 19th International Symposium on Plasma Chemistry (ISPC-19), 26–31 July 2009, Bochum, Germany. Other presentations are published in this issue, pp. 1189–1351.

‡Corresponding author: Tel.: +420-54949 3368; E-mail: lenkaz@physics.muni.cz

molecular dynamic simulations and thermodynamic arguments support the assumption that dissolution and supersaturation of carbon atoms in the particles belong to the steps of SWNT nucleation, similar to those of arc and laser ablation methods [3]. Subsequently, carbon atoms precipitate at the surface in the form of sp^2-bonded carbon structure. The catalysis of CNTs is discussed in more details in the next introductory section.

The CVD techniques can be categorized according to the energy source, gas mixture, and catalyst preparation. In thermal CVD, a carbon-containing gas mixture is heated typically to 550–1100 °C by a conventional heat source such as a resistive or inductive heater, furnace, or IR lamp. Plasma-enhanced CVD (PECVD) modifies this method by the application of an electrical discharge ignited in the gas mixture.

In the literature, one can find various opinions concerning the advantages of PECVD over thermal CVD process for the growth of CNTs. A widely accepted argument in favor of the PECVD growth process is the presence of an inherent electric field influencing the growth orientation of CNTs [4,5]. Indeed, the vertical alignment of nanotubes is very important in many applications. Additionally, some papers support the conventional argument concerning the lower process temperature of PECVD with respect to the thermal CVD. This view is based on the well-known fact that PECVD allows substantially lower wafer temperatures (below 100 °C). Meyyappan and Hash [4,5] argue, on the other hand, that CNT production does not need precursor dissociation in the gas phase, and since it is a catalyzed process with surface reactions occurring at reasonable rates only over 500 °C, it makes very little difference between thermal and plasma CVD from the surface temperature point of view. However, Hofmann [6,7] demonstrated that using the DC glow discharge process, with carefully prepared catalyst NPs, the CNFs can be prepared at temperatures as low as 120 °C. Therefore, it would seem that the conditions for CNTs/CNFs growth are not yet fully understood. It became clear that the former argument for minimum temperatures does not hold, even for thermal CVD, when considering the result of Cantoro et al. [8] which demonstrated a surface-bound CVD growth of SWNTs at temperature of 350 °C.

The most important thermal CVD methods for synthesis of CNTs can be divided into four groups [9]:

- methane or other hydrocarbon CVD,
- carbon monoxide CVD,
- alcohol CVD,
- water-assisted CVD (supergrowth).

In the 1990s, the MWNTs were synthesized by CVD usually using C_2H_4 and C_2H_2. The synthesis of bulk amount of SWNTs using methane CVD was developed by the group of Dai in 1998 [10,11]. Mass production of SWNTs by high-pressure decomposition of CO on metal NPs was demonstrated by Smalley's group [12,13].

The CVD methods are often limited by the low activity and short lifetime of the catalyst. The dead catalysts remain in the as-grown material as impurities. Synthesis of high-purity long SWNTs using alcohols (CH_3OH, C_2H_5OH) showed the importance of OH radicals [14]. These radicals, formed at high temperature from alcohol, suppress the poisoning of catalyst by removal of amorphous carbon. A dramatic improvement was obtained by the addition of water vapor. Water-stimulated enhanced catalytic activity resulted in massive growth of the SWNT forest, leaving the catalyst particles on the substrate, i.e., so-called root growth of CNTs [15]. Although aligned, the SWNTs occupied only 3.6 % of the total volume and, therefore, diffusion did not limit their growth.

PECVD has many variants, differing by the type of discharge and gas mixture. Non-equilibrium (low-temperature) discharges at low pressures, such as MW [16], MW electron-cyclotron resonance (ECR) [17] and DC glow discharges [6,7,18,19], capacitive [20,21] or inductive [22–24] radio-frequency (RF) glow discharges, have previously been applied for the deposition of MWNTs. Due to the plentiful supply of carbon caused by the presence of reactive radicals and unsaturated hydrocarbons in

plasma, ion damage, and probably also unsuitable catalyst preparation, many of the PECVD processes were not successful in the synthesis of SWNTs. However, it has been shown, in some recent publications, that the low-pressure PECVD process is capable of yielding SWNTs [25–27].

Recently, atmospheric-pressure discharges have been studied for the synthesis of CNTs because their experimental set-ups do not require expensive vacuum systems. With regards to the dielectric barrier discharges (DBDs), Kyung, Lee et al. investigated filamentary DBD discharges at kHz frequencies for the deposition of supported CNTs. Their investigations were carried out using a multipin electrode covered by a dielectric plate [28] and capillary dielectric barrier [29–31] configurations. The most successful application of DBD, in this case its glow mode (atmospheric-pressure glow), was performed by Nozaki et al. It has been shown that vertically aligned SWNTs grow in RF atmospheric-pressure glow (APG) discharge using $He/H_2/CH_4$ feed [32]. This result revealed the importance of a catalyst NP preparation for the achievement of SWNTs because Nozaki et al. reported formerly the growth of unaligned CNTs of low quality in APG driven at 125 kHz [33] and the growth of CNFs in RF APG [34].

Arc jets or torches offer quite different plasma properties than "cold" DBD discharges. The DC plasma arc jet or torch ignited in flowing gas between two electrodes can be used for the synthesis of CNTs in the conditions similar to the arc discharge method. The experiments are based on the evaporation of solid carbon introduced as one of the electrodes and/or powder [35,36]. The catalyst can be integrated into the graphite electrode or introduced into the gas phase. Generally, these methods produce soot with a certain portion of unaligned single- and multi-walled CNTs.

Several experiments with microwave (MW) torches have been focused on the floating catalyst approach using vapors of ferrocene or iron pentacarbonyl. Therefore, it also resulted in bulk production of unaligned CNTs [37,38]. However, we have shown that MW torch is capable of the high-speed synthesis of vertically aligned supported CNTs [39–41]. This paper provides a critical overview of the previous experiments, supplemented by recent improvements of the torch design and deposition procedure, discharge diagnostics, the study of catalyst phase, and effects of underlaying material.

CATALYSTS IN CHEMICAL VAPOR DEPOSITION OF CARBON NANOTUBES

The introduction of a catalyst divides the CVD methods into the floating catalyst methods group, using a catalyst in the gas phase, and the surface-bound techniques group with supported catalyst. In the former method, the metal- and carbon-containing vapors are mixed in order to synthesize CNTs. Usually, a metallocene-hydrocarbon solution, most commonly ferrocene dissolved in benzene or ether, is injected into a suitable furnace [42–45]. In almost all cases, the nanotubes are grown on quartz (SiO_2), in the form of either a specific substrate or the reactor wall. Zhang et al. reported that aligned CNTs grow only on SiO_2 substrates and not Si [46].

The surface-bound CVD method utilizes the catalyst NPs supported by the substrate [47], ultrathin films deposited on flat substrates [48–53] or ultrathin films deposited on powder and/or porous materials [12,54–56]. The key factor is to perform effectively the restructuring of the ultrathin metallic film into active catalytic NPs. The size of these particles and the carbon-containing gas used for the growth of CNTs determine the final distribution of CNT diameters [57,58] and morphologies of CNTs/CNFs [8,59]. The nature of the catalyst surface is crucial especially at low temperatures, where surface diffusion is assumed to be the predominant mechanism [8,60,61]. Therefore, the growth of CNTs is preceded by high-temperature processing of metallic film that varies depending on the particular procedure in use.

The restructuring of ultrathin metallic films for the catalysis of CNT growth is usually obtained by heating the films in N_2, H_2, or NH_3 [62–64] or plasma treatment [65–68]. Thin films have a high surface-to-volume ratio, and the heating results in the development of holes and, eventually, particles [69]. The particles can coalesce during continuous heating due to Ostwald ripening or surface migration [70–72], thus modifying the final distribution of catalyst particles. This process is strongly dependent on the heating time and gas environment [63,73,74], the thickness of the pristine catalytic layer

[61,73,75,76] and its surface morphology [77]. In addition to this, the interaction with the material under the catalyst is of importance especially in the case of integration on the Si substrates. At temperatures of CNT growth, the metal catalyst can react with the Si substrate and the catalytic particles change from pure metal to metal silicide. It is still a matter of debate as to how the formation of metal silicides affects particle catalytic activity [62].

It was found that application of a buffer layer between the Si-supporting substrate and metal catalyst significantly improves the catalytic function of the created particles and consequently the CNT growth because the formation of metal silicides is suppressed [78]. The material of the buffer layer varied from the frequently used SiO_2 [73,74] to TiN [78]. The influence of several different buffer layers was compared by Arcos et al. [79]. Recently, Mattevi et al. studied chemical interactions of SiO_2-supported Fe catalyst films during acetylene exposure in the temperature range 400–600 °C [80]. A rapid transition from an initially chemisorbed carbon on metallic Fe particles to a sp^2 graphitic carbon network was observed through the formation of an intermediate carbidic stage. Pretreatment of the Fe catalytic film by hydrogen beam sputtering influenced the initial catalyst de-wetting and increased the CNT yield.

A large section of CNT applications require nanotubes attached and grown directly on conductive substrates. However, the growth of CNTs on conductive Si would appear to be difficult for some CVD procedures. Esconjauregui et al. [62] compared CNT catalysis for annealed Ni and Co films sputtered on thermal SiO_2 and bare Si. It was found that metal silicide as the catalyst on Si substrate can only be used in a narrow process window, otherwise NPs sinter or become embedded before CNT growth occurs.

Detailed analyses of CNT films, grown by thermal CVD in acetylene/hydrogen mixture on Si wafers with Fe catalytic film, have been reported by Yao et al. [81–83]. Fe ultrathin film was restructured by heat treatment in Ar/H_2 and, thereby, nanosized particles of $(Fe,Si)_3O_4$ were formed. Significant differences in the evolution of the particles, i.e., their composition and structure, and CNT growth were observed for CVD at 900 and 750 °C. At 900 °C, synthesized CNTs were sparsely distributed on the supporting substrate and the particles were reduced to catalytic iron silicides, α-(Fe,Si). A low amount of iron carbides Fe_7C_3 was also detected. At 750 °C, densely aligned CNTs were synthesized perpendicularly to the substrate. It was correlated with a refinement of $(Fe,Si)_3O_4$ particles, leading to the formation of fine Fe- and Si-containing particles. It was observed that an initial random CNT growth was followed by an aerosol growth of aligned nanotubes. This resulted in a two-layered film structure, where a film of aligned nanotubes is lifting the initially formed nanotube network from the substrate [83].

A question, requiring further discussion, concerns the oxidation state and thickness of the oxide layer on the catalyst. Metal surfaces and their oxidation have been extensively investigated in situ under UHV/HV conditions [84] and in an oxidizing atmosphere [85], respectively. However, the applications of metal films as catalysts for the synthesis of CNTs reveal the necessity to study their oxidation after exposure to air and subsequent activation for the CNT growth by calcination in different gas environments or by interaction with different plasmas. It was demonstrated by Arcos et al. [86] that oxidized Fe NPs on Al_2O_3 buffer layer exhibited much better catalytic activity than metallic, although the metallic particles are efficient catalysts on other substrates, such as TiN or TiO_2.

RESULTS AND DISCUSSION

Design of MW torch and its present improvement

The apparatus consisted of an MW generator, working at a frequency of 2.45 GHz, with a standard rectangular waveguide, transmitting the MW power through a coaxial line to a hollow nozzle electrode. Ferrite circulator protected the generator from the reflected power by re-routing it to the water load. Matching of the plasma load to the line impedance was achieved by a combination of a movable short

plunger and a line stretcher as described in [39]. The coaxial line and the nozzle electrode accommodated a dual gas flow. The central conductor of the coaxial line was held in place by boron nitride ceramics. The outer conductor was terminated by a flange. The standard deposition mixture consisted of argon (700–1500 sccm), methane (42 sccm), and hydrogen (285–430 sccm). Argon passed through the center, whereas methane/hydrogen passed through the outer housing.

Recent optimization of the MW torch design led to few improvements as compared to the previously published papers [39–41]. A stub tuner was mounted to the waveguide for easiest load matching, and the design of the torch was modified in order to achieve better stability of torch discharge. The reactive mixture of CH_4/H_2 was added by a concentric opening instead of the set of holes in the outer housing. The plasma torch was enclosed by a quartz tube, 200 mm in length, with a duralumin shielding wrapped around the tube. The diameter of the quartz tube was increased from the originally 40 to 80 mm. A detailed drawing of the current set-up is in Fig. 1.

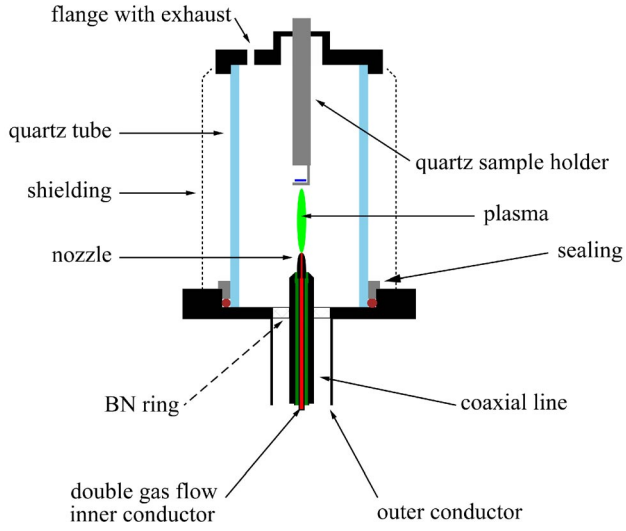

Fig. 1 Set-up of the MW torch deposition chamber.

Deposition of CNTs and approaches improving their uniformity

The substrate for MWNT growth, a piece of Si with dimensions 10 × 15 mm^2, was fixed on the quartz holder at the variable distance from the torch nozzle. It was heated by a heat exchange with hot gas and surface recombination. The deposition temperature was 700 °C. The catalyst, used for the deposition of CNTs, was 5–15-nm-thick Fe film prepared by vacuum evaporation. If not specified otherwise, the Fe film was deposited on SiO_x barrier layer prepared by PECVD on the Si substrate in low-pressure RF capacitively coupled discharge from a mixture of hexamethyldisiloxan (HMDSO) and oxygen. The RF (13.56 MHz) power applied for the deposition was 100 W. The pressure in the reactor and the percentage of HMDSO in the mixture were 5 Pa and 20 %, respectively.

The CNTs were investigated using a field emission scanning electron microscope (FE-SEM) JOEL 6700F with three different electron detectors. The conventional E-T scintillation PMT system mounted aside from the electron beam detected all the electrons producing a lower electron image (LEI). The second system detected true secondary electrons at the semi-in-lens position, i.e., in the direction of the objective lens, producing a highly resolved secondary electron image (SEI). The third detector (AUX1), the yttrium-aluminum-garnet (YAG) single-crystal scintillator at the semi-in-lens position, collected back-scattered electrons. The SEI micrographs provided quality, highly resolved images.

Therefore, they were often used for detailed studies of CNTs. The LEI and AUX1 micrographs provide less resolved images with partial information about distribution of different elements because heavier elements appear brighter. They were used to distinguish carbon material from the Fe catalyst.

The disadvantage of the torch-deposited CNTs, shown in our earlier experiments, consisted in the nonuniformity of deposit caused by spatial nonuniformity of the discharge and substrate heating [40]. The deposition was carried out without any separate pretreatment of the catalytic layer and the substrate side with catalyst faced the torch. The HRSEM images were analyzed with respect to the distribution of CNTs and Fe-NPs diameters. The areas with densely aligned CNTs contained nanotubes with an average diameter of 38 nm and Fe-NPs of similar size at the tips. At the edges of these areas, larger particles with a diameter of about 80 nm were covered by sparsely distributed CNTs of diameter 10–17 nm. In an intermediate region, relatively thin CNTs elevated much larger catalytic particles. Therefore, these results pose a question of the mechanism of nanotube growth that did not required catalyst pretreatment discussed in the introductory section and, in some parts of the substrate, resulted in a different sizes of nanotubes and catalytic particles.

Jasek et al. [41] discussed a procedure improving the deposition uniformity, leading to the nanotubes and catalytic particles of similar sizes. This was achieved by heating the substrate prior to the deposition in H_2/Ar plasma of the torch. The dense, well-aligned CNTs with a length of 100 m were obtained after 3 min of H_2/Ar plasma treatment followed by 15 min of the deposition in CH_4/H_2/Ar. TEM micrographs revealed that the CNTs had a wide range of diameters from 30 to 100 nm as the result of too lengthy preheating time, leading to coagulation of small NPs. Additionally, the deposition time, as long as 15 min, resulted in a catalyst poisoning effect with a subsequent deposition of an amorphous carbon layer [41].

The catalyst poisoning was caused by the high density of the dissociated carbon species reaching the substrate. Therefore, the treatment and the deposition time were shortened in the present experiments. A quite uniform forest of 20-μm-long nanotubes was obtained using 30 s of H_2/Ar plasma treatment followed by 30 s of deposition in CH_4/H_2/Ar mixture. The edge of the CNT forest imaged by laser confocal microscope Olympus LEXT OLS 3100 is shown in Fig. 5. Additionally, a different procedure for the uniform deposition of CNTs was explored. The substrate side with the catalyst was placed outwards of the torch. In this case, the CNTs were grown by a speed and density similar to those of the catalyst faced the torch and the whole area was covered by a uniform deposit.

Diagnostics of the deposition process

The gas temperature of the active discharge reached approximately 4000 °C and, therefore, the discharge was capable of heating the substrate to a deposition temperature of about 700 °C without an external heater. The spatial radial profile of the gas temperature, 10 mm from the nozzle, is shown in Fig. 2. It was determined from fitting the (0,0) rotational emission band of the C_2 Swan system because, at the atmospheric pressure, the rotational temperature approximates very well the temperature of gas. The radial profile was obtained by Abel transform of spatially resolved measurements.

Therefore, its temperature was determined by power input, gas mixture, and its distance from the nozzle. The MW power applied for the deposition of CNTs was 400 W. The substrate temperature, measured by a Raytek Thermalert TX pyrometer, as a function of the substrate distance from the nozzle is given in Fig. 3. The plotted values were determined after 50 s of temperature stabilization. The CNT growth experiments started with the ignition of the discharge in pure Ar and positioning the substrate at the desired distance from the nozzle. Then, CH_4 and H_2 electronic mass flow controllers were opened. Due to the low heat capacity of the substrate, the temperature rapidly increased from the starting room temperature to the deposition temperature as shown in Fig. 4. The intermediate period of temperature fluctuation was caused by positioning the substrate in front of the Ar plasma torch. It can be seen from the figure that the increased temperature, caused by CH_4/H_2 presence in the discharge, had

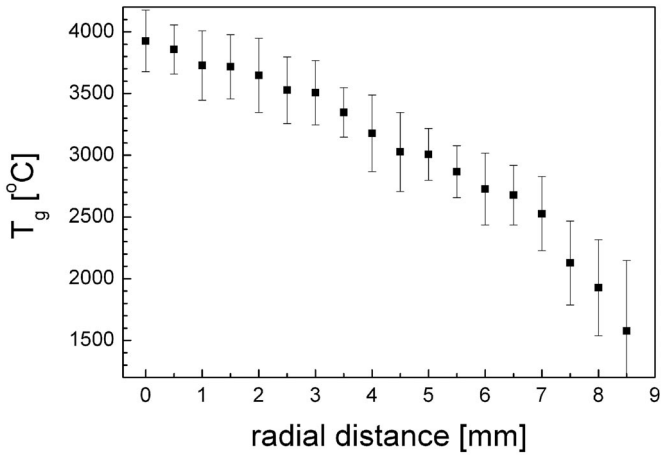

Fig. 2 Radial profile of gas temperature 10 mm from the nozzle for 42/430/800 sccm of $CH_4/H_2/Ar$ and power of 400 W.

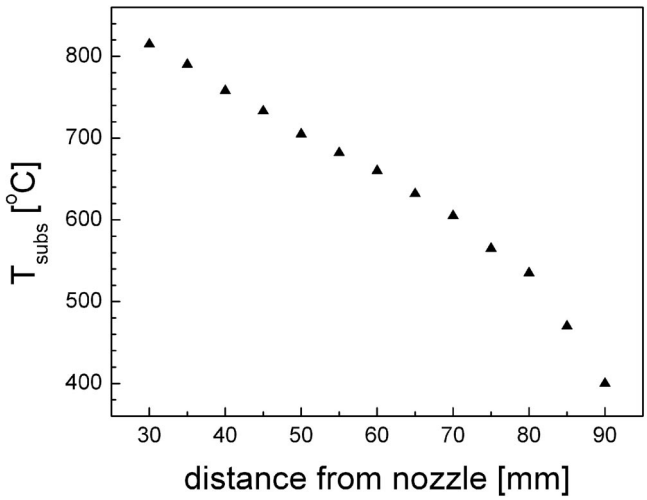

Fig. 3 Substrate temperature achieved by heating the Si substrate in MW torch at different distances from the torch nozzle. For flow rate and power, see caption of Fig. 2.

a delay of about 10 s related to a delay between the opening of the flow controllers and actual CH_4/H_2 admixing. As in many previous experiments [39,40], a disintegration of thin Fe catalytic film into NPs was an integral part of the deposition process with the beginning period of about 15 s during which the Fe film was exposed only to the Ar discharge.

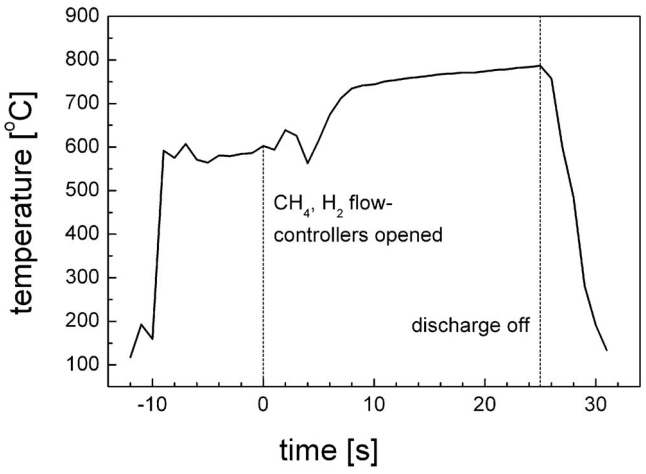

Fig. 4 Evolution of the substrate temperature during the beginning of the deposition process and after discharge shut down.

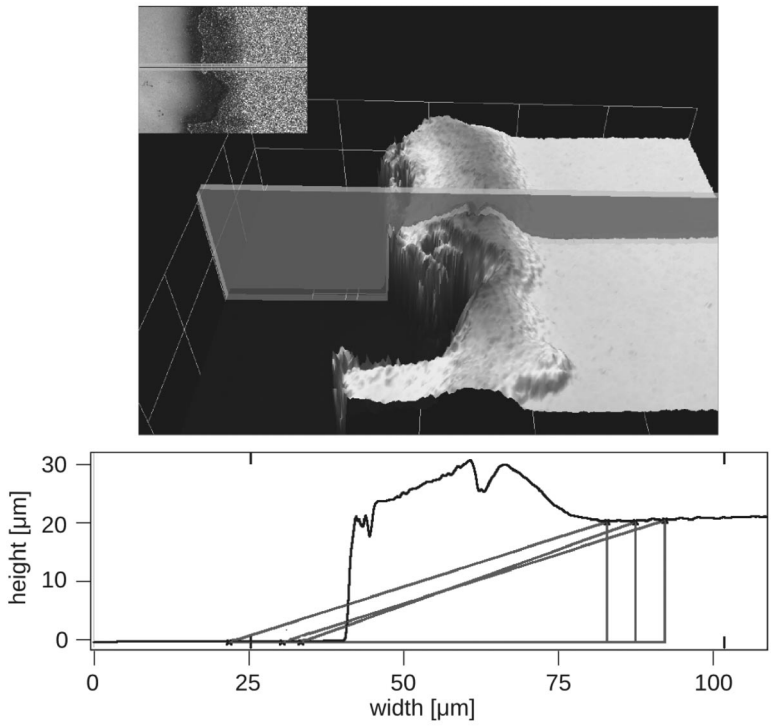

Fig. 5 The edge of CNT forest imaged by laser confocal microscope: overview image (top) and its cross-section (bottom). The substrate with 15-nm-thick Fe film was plasma treated for 30 s in H_2/Ar and CNTs were then deposited for 30 s in CH_4/H_2/Ar mixture (42/430/1500 sccm) at 700 °C.

Study of catalyst phase and effect of underlaying material

The phase of Fe catalyst and its transformation after plasma synthesis of CNTs were studied by Mössbauer spectroscopy. For this purpose, 10-nm-thick films of enriched ^{57}Fe (90 at. %) were vacuum

evaporated on the Si/SiO_x substrates standardly used before. ^{57}Fe Mössbauer spectra were measured using detection of conversion electrons with the information depth of about 200 nm and calibrated against α-Fe as the standard. The conversion electron Mössbauer spectra (CEMS) of the as-prepared $Si/SiO_x/Fe$ sample showed that Fe film is oxidized because the signal corresponded solely to Fe^{3+} ions. After 1 min plasma growth of nanotubes in $CH_4/H_2/Ar$ at a temperature of 700 °C, the catalytic particles, found on the top of CNTs, were in the form of Fe carbides, Fe_3C, Fe_5C_2, and amorphous $Fe_{5-x}C_{2+x}$. Besides these major constituents, traces of reduced γ-Fe and iron oxide (Fe^{3+} ions) were also detected. The results, therefore, confirm the model of CNT growth based on carbon dissolution in the catalyst.

As mentioned in the introduction, a barrier layer between the Si substrate and catalytic thin film is often required for the growth of good-quality CNTs. However, there are some applications in which electrical contact between the Si substrate and CNTs is necessary and a dielectric barrier layer, such as Si oxide, cannot be used. CNTs grown by MW torch were used as electron-emitting electrode of the gas pressure sensor [87]. In this case, Fe film was evaporated on highly doped Si (specific resistance of 0.005 Ωm) rinsed in hydrofluoric acid immediately before the Fe deposition. Therefore, there was only a very thin native oxide between the Si and the evaporated Fe. Despite this, the CNTs were grown again in the form of dense nanotubes aligned by crowding effect (Fig. 6).

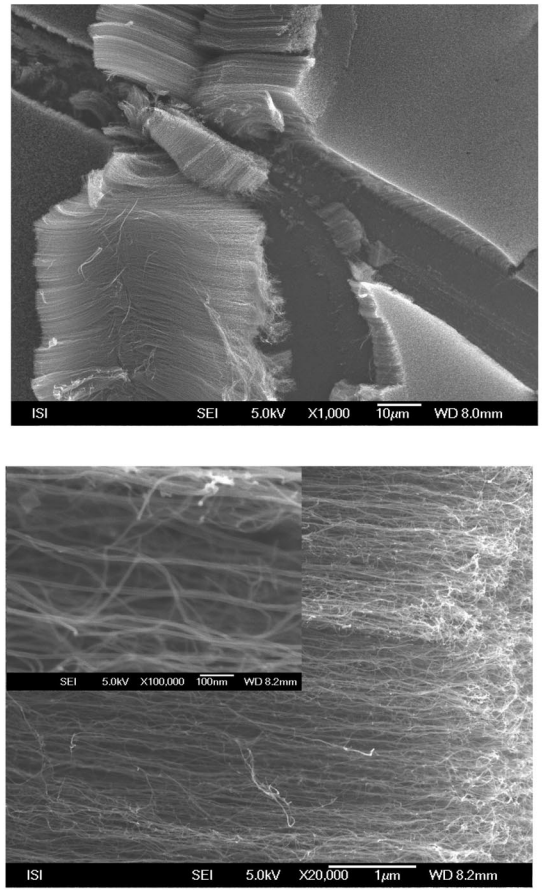

Fig. 6 SEM micrographs of CNTs deposited on Si without SiO_x barrier layer: low-resolution image of a tweezers-made scratch into the CNTs forest (top) and higher magnification side view images (bottom). CNTs were deposited 45 s in 42/430/1500 sccm of $CH_4/H_2/Ar$ at temperature of 700 °C.

The CNTs grown in MW torch were also intended to create a gas sensor based on the changes of electrical resistance measured between two planar electrodes connected by CNTs. Although CNTs were organized perpendicular to the substrate by the crowding effect, as revealed by any side view into an artificially made scratch of the CNTs forest, a magnified top view showed their mutual interconnection (Fig. 7). Then, the fabrication of the gas sensor required local contacts to such mesh of CNTs. Therefore, the CNTs were grown on a SiO_x dielectric layer and gold contacts were vacuum evaporated before the Fe film or after the growth of CNTs. The former approach revealed that only sparsely distributed nanotubes grow on the stack of $Si/SiO_x/Au/Fe$ (Fig. 8) due to an interaction of gold with iron. It resulted in poor, unreliable electrical contacts to the CNT mesh not suitable for sensor fabrication. The latter approach, i.e., evaporation of gold contacts on the top of the sensor, resulted in better reproducibility of the resistance, yielding the relative error of 15 % for the 23 tested sensors.

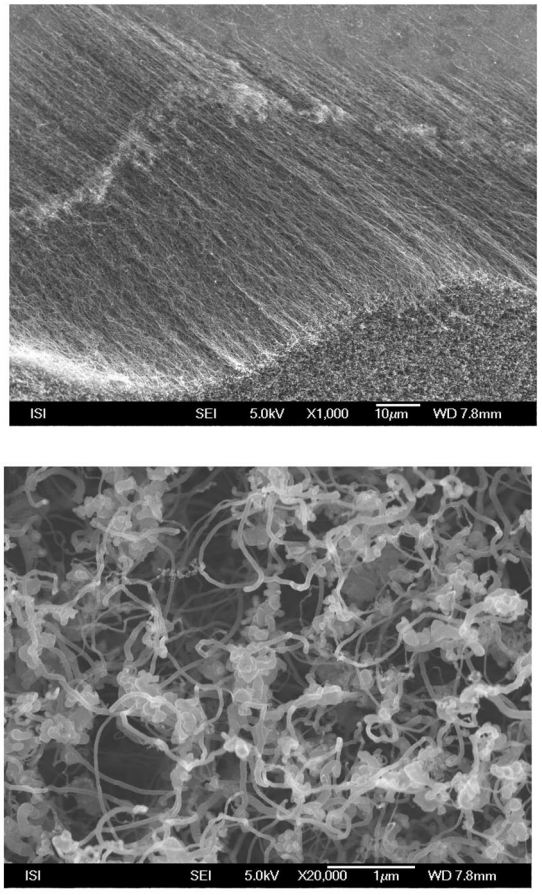

Fig. 7 Side and top view SEM micrographs of CNTs deposited 90 s on $Si/SiO_x/Fe$ in 42/430/800 sccm of $CH_4/H_2/Ar$ at temperature of 700 °C.

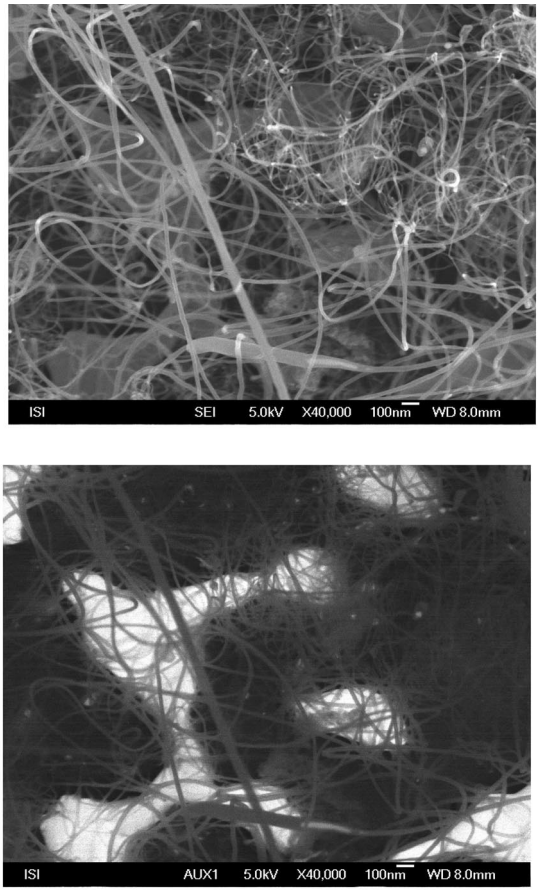

Fig. 8 SEM micrographs of CNTs deposited 90 s on Si/SiO_x/Au/Fe in 42/430/1500 sccm of CH_4/H_2/Ar at temperature of 700 °C: image in true secondary (top) and back-scattered (bottom) electrons.

CONCLUSION

The growth processes and applications of CNTs establish encouraging results for current advances in nanotechnologies. There are many different techniques for CNT synthesis, and plasma technologies find a hard competitor in thermal CVD processes. The particular process is, therefore, selected according to the requirements of the application. For the development of composites and other structural applications, the merit is the ability to produce large amounts at a reasonable price. In contrast, the ability to achieve controlled growth (of a specified thickness) on patterns is important for applications in nanoelectronics, field emission, displays, and sensors.

This contribution discusses the method for synthesis of CNTs using atmospheric-pressure MW torch. It was successfully applied to the fast deposition of MWNTs on the substrate without necessity of any vacuum or heating equipment. Dense straight-standing nanotubes were prepared on Si substrates with and even without a barrier SiO_x layer. Therefore, it was possible to produce CNTs directly on conductive Si and to use them as electron-emitting electrodes of the gas pressure sensor. The CNTs grown in MW torch were also intended to create a gas sensor based on the changes of electrical resistance measured between two planar electrodes connected by CNTs. Although CNTs were organized perpendicular to the substrate by the crowding effect, as revealed by the SEM side view into an artificially made scratch of the CNT forest, the magnified top view showed their mutual interconnection.

ACKNOWLEDGMENTS

This work was supported by the Czech Ministry of Education under the project MSM 0021622411, by the Grant Agency of the Czech Republic, contracts P205/10/1374, 202/08/0178, and 104/09/H080 by the Academy of Sciences of the Czech Republic, contract KAN311610701. The authors are grateful to Jirina Matejkova for scanning electron microscopy of CNTs.

REFERENCES

1. M. Meyyappan (Ed.). *Carbon Nanotubes, Science and Applications*, CRC Press, Boca Raton (2005).
2. V. Vinciguerra, F. Buonocore, G. Panzera, L. Occhipinti. *Nanotechnology* **14**, 655 (2003).
3. F. Ding, K. Bolton. *Nanotechnology* **17**, 543 (2006).
4. M. Meyyappan, L. Delzeit, A. Cassell, D. Hash. *Plasma Sources Sci. Technol*. **12**, 205 (2003).
5. D. B. Hash, M. Meyyappana. *J. Appl. Phys*. **93**, 750 (2003).
6. S. Hofmann, C. Ducati, J. Robertson. *Appl. Phys. Lett*. **83**, 135 (2003).
7. S. Hofmann, C. Ducati, B. Kleinsorge, J. Robertson. *Appl. Phys. Lett*. **83**, 4661 (2003).
8. M. Cantoro, S. Hofmann, S. Pisana, V. Scardaci, A. Parvez, C. Ducati, A. Ferrari, A. M. Blackburn, K.-Y. Wang, J. Robertson. *Nanolett*. **6**, 1107 (2006).
9. A. Jorio, G. Dresselhaus, M. Dresselhaus (Eds.). *Carbon Nanotubes: Advanced Topics in the Synthesis, Structure, Properties and Applications*, Springer (2008).
10. J. Kong, H. Soh, A. Cassell, C. Quate, H. Dai. *Nature* **395**, 878 (1998).
11. J. Kong, A. Cassell, H. Dai. *Chem. Phys. Lett*. **292**, 567 (1998).
12. H. Dai, A. Rinzler, P. Nikolaev, A. Thess, D. Colbert, R. Smalley. *Chem. Phys. Lett.* **260**, 471 (1996).
13. J. Hafner, M. Bronikowski, B. Azamian, P. Nikolaev, A. Rinzler, D. Colbert, K. Smith, R. Smalley. *Chem. Phys. Lett*. **296**, 195 (1998).
14. S. Maruyama, R. Kojima, Y. Miyauchi, S. Chiashi, M. Kohno. *Chem. Phys. Lett.* **360**, 229 (2002).
15. K. Hata, D. Futaba, K. Mizuno, T. Namai, M. Yumura, S. Iijima. *Science* **306**, 1362 (2004).
16. J. Gao, K. Umeda, K. Uchino, H. Nakashima, K. Muraoka. *Mater. Sci. Eng*. **352**, 308 (2003).
17. C. Hsu, C. Lin, H. Chang, C. Kuo. *Thin Solid Films* **420–421**, 225 (2002).
18. J.-H. Han, T. Lee, J.-B. Yoo, C.-Y. Park, T. Jung, J. Kim, S. Yu, W. Yi. *J. Vac. Sci. Technol. B* **21**, 1720 (2003).
19. I. Obraztsov, A. Zolotukhin, A. Volkov, Y. Svirko. *Carbon* **41**, 836 (2002).
20. B. O. Boskovic, V. Stolojan, R. Khan, S. Haq, S. Silva. *Nat. Mater*. **1**, 165 (2002).
21. C. Lin, I. C. Leu, J. Yen, M. Hon. *Nanotechnology* **15**, 176 (2003).
22. L. Delzeit, I. McAninch, B. Cruden, D. Hash, B. Chen, J. Han, M. Meyyappan. *J. Appl. Phys.* **91**, 6027 (2002).
23. L. Delzeit, C. Nguyen, R. Stevens, J. Han, M. Meyyappan. *Nanotechnology* **13**, 280 (2002).
24. I. Denysenko, S. Xu, J. Long, P. Rutkevych, N. Azarenkov, K. Ostrikov. *J. Appl. Phys.* **95**, 2713 (2004).
25. T. Kato, G. Jeong, T. Hirata, R. Hatakeyama, K. Tohji, K. Motomiya. *Chem. Phys. Lett.* **381**, 422 (2003).
26. T. Kato, R. Hatakeyama, K. Tohji. *Nanotechnology* **17**, 2223 (2006).
27. T. Iwasaki, G. Zhong, T. Aikawa, T. Yoshida, H. Kawarada. *J. Phys. Chem. B* **109**, 19556 (2005).
28. Y.-H. Lee, S.-H. Kyung, C.-W. Kim, G.-Y. Yeom. *Carbon* **44**, 799 (2006).
29. S.-J. Kyung, Y.-H. Lee, C.-W. Kim, J.-H. Lee, G.-Y. Yeom. *Carbon* **44**, 1530 (2006).
30. S.-J. Kyung, Y.-H. Lee, C.-W. Kim, J.-H. Lee, G.-Y. Yeom. *Thin Solid Films* **506–507**, 268 (2006).

31. S.-J. Kyung, M. Voronko, Y.-H. Lee, C.-W. Kim, J.-H. Lee, G.-Y. Yeom. *Surf. Coat. Technol.* **201**, 5378 (2007).
32. T. Nozaki, K. Ohnishi, K. Okazaki, U. Kortshagen. *Carbon* **45**, 364 (2007).
33. T. Nozaki, Y. Kimura, K. Okazaki. *J. Phys. D: Appl. Phys*. **35**, 2779 (2002).
34. T. Nozaki, T. Goto, K. Okazaki, K. Ohnishi, L. Mangolini, J. Heberlein, U. Kortshagen. *J. Appl. Phys*. **99**, 024310 (2006).
35. H. Takikawa, M. Ikeda, K. Hirahara, Y. Hibi, Y. Tao, P. A. Ruiz, T. Sakakibara, S. Itoh, S. Iijima. *Physica B* **323**, 277 (2002).
36. R. H. Amirov, E. I. Asinovsky, E. K. Isakaev, V. I. Kiselev. *High Temp. Mater. Process.* **10**, 197 (2006).
37. O. Smiljanic, B. Stanseld, J.-P. Dodelet, A. Serventi, S. Désilets. *Chem. Phys. Lett.* **356**, 189 (2002).
38. C.-K. Chen, W. L. Perry, H. Xu, Y. Jiang, J. Phillips. *Carbon* **41**, 2555 (2003).
39. L. Zajíčková, M. Eliáš, O. Jašek, V. Kudrle, Z. Frgala, J. Matějková, J. Buršík, M. Kadlečíková. *Plasma Phys. Control. Fusion* **47**, B655 (2005).
40. L. Zajíčková, M. Eliáš, O. Jašek, Z. Kučerová, P. Synek, J. Matějková, M. Kadlečíková, M. Klementová, A. Vojačková. *Plasma Process. Polym*. **4**, S245 (2007).
41. O. Jašek, M. Eliáš, L. Zajíčková, Z. Kučerová, J. Matějková, A. Rek, J. Buršík. *J. Phys. Chem. Solids* **68**, 738 (2007).
42. P. Nikolaev, M. Bronikowski, R. Bradley, F. Rohmund, D. Colbert, K. Smith, R. Smalley. *Chem. Phys. Lett*. **313**, 91 (1999).
43. H. Zhu, C. Xu, D. Wu, B. Wei, R. Vajtai, P. Ajayan. *Science* **296**, 884 (2002).
44. W. Ren, F. Li, J. Chen, S. Bai, H.-M. Cheng. *Chem. Phys. Lett.* **359**, 196 (2002).
45. C. Singh, M. S. Shaer, A. H. Windle. *Carbon* **41**, 359 (2003).
46. Z. J. Zhang, B. Q. Wei, G. Ramanath, P. M. Ajayan. *Appl. Phys. Lett*. **77**, 3764 (2000).
47. Y. Li, W. Kim, Y. Zhang, M. Rolandi, D. Wang, H. Dai. *J. Phys. Chem*. **105**, 11424 (2001).
48. S. Hofmann, M. Cantoro, B. Kleinsorge, C. Casiraghi, A. Parvez, J. Robertson, C. Ducati. *J. Appl. Phys.* **98**, 034038 (2005).
49. C. Emmenegger, J.-M. Bonard, P. Mauron, P. Sudan, A. Lepora, B. Grobety, A. Zuttel, L. Schlapbach. *Carbon* **41**, 539 (2003).
50. C. Lee, D. Kim, T. Lee, Y. Choi, Y. Park, Y. Lee, W. Choi, N. Lee, G.-S. Park, J. Kim. *Chem. Phys. Lett*. **312**, 461 (1999).
51. C. Lee, J. Park, S. Kang, J. Lee. *Chem. Phys. Lett*. **323**, 554 (2000).
52. C. Lee, J. Park, J. Park. *Chem. Phys. Lett.* **323**, 560 (2000).
53. P. Mauron, C. Emmenegger, A. Züttel, C. Nützedel, P. Suden, L. Schlabach. *Carbon* **40**, 1339 (2002).
54. J. J. Kong, A. M. Cassell, H. Dai. *Chem. Phys. Lett*. **292**, 567 (1998).
55. P. Mauron, C. Emmenegger, P. Sudan, P. Wenger, S. Rentsch, A. Züttel. *Diamond Relat. Mater*. **12**, 780 (2003).
56. M. Jose-Yacaman, M. Miki-Yoshida, L. Rendon, J. Santiesteban. *Appl. Phys. Lett*. **62**, 657 (1993).
57. H. Dai. *Surf. Sci*. **500**, 218 (2002).
58. O. A. Nerushev, S. Dittmar, R. E. Morjan, F. Rohmund, E. E. B. Campbell. *J. Appl. Phys.* **93**, 4185 (2003).
59. C. L. Cheung, A. Kurtz, H. Park, C. M. Lieber. *J. Phys. Chem. B* **106**, 2429 (2002).
60. S. Helveg, C. López-Cartes, J. Sehested, P. L. Hansen, B. S. Clausen, J. R. Rostrup-Nielsen, F. Abild-Pedersen, J. K. Norskov. *Nature* **427**, 426 (2004).
61. S. Hofmann, G. Csányi, A. C. Ferrari, M. C. Payne, J. Robertson. *Phys. Rev. Lett.* **95**, 1 (2005).
62. S. Esconjauregui, C. M. Whelan, K. Maex. *Nanotechnology* **18**, 015602 (2007).
63. H. Liu, G.-A. Cheng, R. Zheng, Y. Zhao, C. Liang. *Surf. Coat. Technol*. **202**, 3157 (2008).

64. J. H. Choi, T. Y. Lee, S. H. Choi, J.-H. Han, J.-B. Yoo, C.-Y. Park, T. Jung, S. Yu, W. Yi, I. T. Han, J. M. Kim. *Thin Solid Films* **435**, 318 (2003).
65. M. S. Kabir, R. E. Morjan, O. A. Nerushev, P. Lundgren, S. Bengtsson, P. Enokson, E. E. B. Campbell. *Nanotechnology* **16**, 458 (2005).
66. Z. F. Ren, Z. P. Huang. *Science* **282**, 1105 (1998).
67. S. H. Tsai, C. W. Chao, C. L. Lee, H. C. Shih. *Appl. Phys. Lett*. **74**, 3462 (1999).
68. M. Okai, T. Muneyoshi, T. Yaguchi, S. Sasaki. *Appl. Phys. Lett*. **77**, 3468 (2000).
69. E. Jiran, C. V. Thompson. *Thin Solid Films* **208**, 23 (1992).
70. J. Wen, J. W. Evans, M. C. Bartelt, J. W. Burnett, P. A. Thiel. *Phys. Rev. Lett*. **76**, 652 (1996).
71. M. Liehr, H. Lefakis, F. K. LeGoues, G. W. Rublo. *Phys. Rev. B* **33**, 5517 (1986).
72. P. R. Gadkari, A. P. Warren, R. M. Todi, R. V. Petrova, K. R. Coey. *J. Vac. Sci. Technol. A* **23**, 1152 (2005).
73. M. Jung, K. Eun, J. Lee, Y. Baik, K. Lee, J. Wan Park. *Diamond Relat. Mater*. **10**, 1235 (2001).
74. S. Pisana, M. Cantoro, A. Parvez, S. Hofmann, A. C. Ferrari, J. Robertson. *Physica E* **37**, 1 (2007).
75. J. Jang, J. Baea, S.-H. Yoon. *J. Mater. Chem*. **13**, 676 (2003).
76. M. Cantoro, S. Hofmann, S. Pisana, C. Ducati, A. Parvez, A. C. Ferrari, J. Robertson. *Diamond Relat. Mater.* **15**, 1029 (2006).
77. H. Liu, G. Cheng, Y. Zhao, R. Zheng, C. Liang, F. Zhao, T. Zhang. *Surf. Coat. Technol.* **201**, 938 (2006).
78. T. de los Arcos, F. Vonau, M. G. Garnier, V. Thommen, H.-G. Boyen, P. Oelhafen, M. Duggelin, D. Mathis, R. Guggenheim. *Appl. Phys. Lett*. **80**, 2383 (2002).
79. T. de los Arcos, M. G. Garnier, P. Oelhafen, D. Mathys, J. W. Seo, C. Domingo, J. Vicente García-Ramos, S. Sánchez-Córtes. *Carbon* **42**, 187 (2004).
80. C. Mattevi, S. Hofmann, M. Cantoro, A. C. Ferrari, J. Robertson, C. Castellarin-Cudia, S. Dola, A. Goldoni, C. Cepek. *Phys. E* **40**, 2238 (2008).
81. Y. Yao, L. K. L. Falk, R. E. Morjan, O. A. Nerushev, E. E. B. Campbell. *J. Mater. Sci.: Mater. Electron.* **15**, 583 (2004).
82. Y. Yao, L. K. L. Falk, R. E. Morjan, O. A. Nerushev, E. E. B. Campbell. *J. Mater. Sci.: Mater. Electron.* **15**, 533 (2004).
83. Y. Yao, L. K. L. Falk, R. E. Morjan, O. A. Nerushev, E. E. B. Campbell. *Carbon* **45**, 2065 (2007).
84. H. Luth. *Solid Surfaces, Interfaces and Thin Films*, Springer (2001).
85. N. Birks, G. Meier, F. Pettit. *Introduction to the High-Temperature Oxidation of Metals*, Cambridge University Press (2006).
86. T. de los Arcos, P. Oelhafen, V. Thommen, D. Mathys. *J. Phys. Chem. C* **111**, 16392 (2007).
87. R. Ficek, M. Eliáš, L. Zajíčková, O. Jašek, R. Vrba. *Applications of Nanotubes and Nanowires*, MRS Proceedings 1018E 1018EE1405 (2007).

